



## Reduced graphene oxide-ZnO hollow microsphere composite for supercapacitor applications



Abqari Luthfi Albert Abdullah<sup>1</sup>, Shahidan Radiman<sup>2</sup>, Wee Siong Chiu<sup>3</sup>,  
Muhammad Azmi Abdul Hamid<sup>2</sup>, Fadhlul Wafi Badrudin<sup>1\*</sup>

<sup>1</sup>Physics Department, Centre for Defence Foundation Studies, Universiti Pertahanan Nasional Malaysia, Malaysia

<sup>2</sup>School of Applied Physics, Faculty of Science and Technology, Universiti Kebangsaan Malaysia, Malaysia

<sup>3</sup>Department of Physics, Faculty of Science, University of Malaya, Malaysia

### Abstract

Through a facile solvothermal synthesis process, a reduced graphene oxide-ZnO microsphere composite was produced at 180 °C for 24 hours. Raman spectroscopy, X-ray diffraction, field emission scanning electron microscopy, and transmission electron microscopy were used to analyze the morphological structures of the material. The analysis revealed that hexagonal phase wurtzite ZnO nanoparticles assembled homogeneous microspheres, decorated on the graphene sheets by graphene oxide functional groups. The ZnO nanoparticles are about 30 nm in size and the microspheres are hollow. A possible growth mechanism for the formation of ZnO hollow microspheres anchored on graphene sheets has been proposed. Cyclic voltammetry, galvanostatic charge-discharge and electrochemical impedance were used to evaluate the electrochemical performance of the composite. At a scan rate of 1 mV/s, the reduced graphene oxide-ZnO hollow microsphere composite electrode demonstrated an enhanced specific capacitance of 40.70 F/g with energy and power densities of 5.75 Wh/kg and 1.97 kW/kg, respectively.

This is an open access article under the [CC BY-SA](https://creativecommons.org/licenses/by-sa/4.0/) license



### Keywords:

Composites;  
Graphene;  
Hollow sphere;  
Solvothermal;  
Zinc oxide;

### Article History:

Received: November 7, 2024  
Received: December 15, 2024  
Accepted: January 19, 2025  
Published: May 17, 2025

### Corresponding Author:

Fadhlul Wafi Badrudin  
Physics Department, Centre for  
Defence Foundation Studies,  
Universiti Pertahanan Nasional  
Malaysia, Malaysia  
Email:  
[fadhlul@upnm.edu.my](mailto:fadhlul@upnm.edu.my)

## INTRODUCTION

Graphene, a two-dimensional atom-thick substance composed of a monolayer hexagonal  $sp^2$ -hybridised carbon, has caught the interest of researchers in recent years due to its unique structure and exceptional electrical, mechanical, thermal, and optical properties [1, 2, 3, 4]. These properties can be enhanced further by fusing graphene sheets with nanoscale or micron-sized transition metal oxides to produce unique graphene-based composites. To achieve exceptional hybrid characteristics in graphene-based composites, a variety of transition metal oxide structures have been linked to graphene layers [5, 6, 7, 8, 9]. Zinc oxide (ZnO), a wide-band gap (3.37 eV) semiconductor, is a transition metal oxide that has drawn considerable research

attention due to its distinctive properties. With a significant exciton binding energy of 60 MeV at ambient temperature, ZnO is a non-toxic, environmentally friendly, and readily available material with cheap production cost. ZnO hollow microspheres are of interest in many technological applications such as solar cells [10], lithium batteries [11], photocatalysis [12], sensors [13], supercapacitor electrode materials [14] and medical [15] because of their low density, high surface area, and hollow geometrical shapes.

Hybridisation of graphene and ZnO structures allows the generation of composites with versatile and tailor-made properties, demonstrating attractive combinations that outperform the individual components [16]. However, the solvothermal synthesis of graphene-

ZnO hollow microsphere composite for supercapacitor applications has received little attention.

In this study, a reduced graphene oxide-zinc oxide hollow microsphere (rGO-ZnO(HMs)) composite was synthesised utilising a solvothermal processing approach. This one-pot synthesis process is straightforward, efficient and requires no reducing or oxidising chemicals. In situ growth of ZnO on the surface of graphene produced uniformly adorned hollow microspheres. The morphological and electrochemical properties of the rGO-ZnO(HMs) composite was thoroughly examined.

## MATERIAL AND METHOD

### Material

Cheap Tubes Inc. provided commercially available graphene oxide (GO, 99 wt%) powder. The GO powder was synthesised using the modified Hummers method. Zinc acetate dihydrate ( $\text{Zn}(\text{CH}_3\text{COO})_2 \cdot 2\text{H}_2\text{O}$ , 99.5%) and absolute ethanol were supplied by Merck and HmbG Chemicals, respectively. No further purification was performed on any of the chemicals and distilled water was used throughout the sample preparation process.

### Solvothermal preparation of rGO-ZnO(HMs) composite

GO powder was dissolved in absolute ethanol to achieve a concentration of 1 mg/ml of GO and stirred continuously for 30 minutes. Subsequently, 2.5 mM of  $\text{Zn}(\text{CH}_3\text{COO})_2 \cdot 2\text{H}_2\text{O}$  was added and the mixture suspension was sonicated for 30 minutes to obtain a homogeneous solution. The suspension was then transferred into a Teflon-lined autoclave. The autoclave was sealed and maintained in the oven at 180 °C for 24 hours. After cooling the autoclave to room temperature naturally, the black precipitates were separated by centrifugation and washed with distilled water and absolute ethanol repeatedly. The pure rGO-ZnO(HMs) composite powder was dried in the oven at 60 °C for 8 hours. For comparison purposes, a control experiment was performed without adding zinc precursor and the product was labeled as rGO.

### Morphological characterisation of rGO-ZnO(HMs) composite

The X-ray diffraction (XRD) spectra on powdered samples was collected via a Bruker D8 Advance 9 Position diffractometer using Cu K- $\alpha$  radiation to determine the crystalline phase of the sample. The disordering of the formed carbon was examined using Raman spectroscopy (Renishaw

inVia system). A field emission scanning electron microscope (FESEM) and a transmission electron microscope (TEM) were used to analyse the structural morphology of rGO-ZnO(HMs) composite.

### Preparation of electrodes and electrochemical characterisation

To evaluate the electrochemical characteristics of the composite, electrodes were prepared by mixing the electroactive materials (rGO and rGO-ZnO(HMs) composite), carbon black and poly(vinylidene fluoride-hexafluoropropylene) (PVDF-HFP) binder at a ratio of 90: 5: 5 by mass. A small quantity of acetone was introduced to the mixture to generate a homogeneous slurry paste, which was subsequently applied onto graphite tape and left to desiccate in an oven at a temperature of 60 °C overnight. A symmetrical electrochemical cell was constructed by placing two identical electrodes with a 25  $\mu\text{m}$  microporous membrane acting as a separator in a 6M KOH electrolyte.

The electrochemical cells were analysed using cyclic voltammetry (CV), galvanostatic charge-discharge (GCD), and electrochemical impedance (EIS) techniques. The analysis was performed utilising a Solartron SI 1286 Electrochemical Interface and a Solartron HF 1255 Frequency Response Analyser. The measurements were conducted at a temperature of 25 °C, which corresponds to room temperature. The CV measurement was performed using a potential range of 0 to 1 V and scan rates ranging from 1 to 100 mV/s. The GCD measurement was performed within a voltage range of 0 to 1 V and at a current density ranging from 0.1 to 1.0 A/g. EIS data were recorded at 10 mV over a frequency range of 10 mHz to 1 MHz.

## RESULTS AND DISCUSSION

### Morphological characteristics

The XRD patterns of the GO, rGO, and rGO-ZnO(HMs) composite are shown in Figure 1(a). The occurrence of oxygenated functional groups linked to the basal planes and edges of carbon sheets is connected to the peak that appears at around 10.8° in the GO pattern [17]. Furthermore, the emergence of minor protrusions at angles of 23.5° and 42.8° in the rGO pattern confirms the reduction of GO to rGO, or reduced graphene oxide [18]. These bumps indicate the removal of a significant number of oxygen-containing groups and the formation of much more disordered graphene sheets.

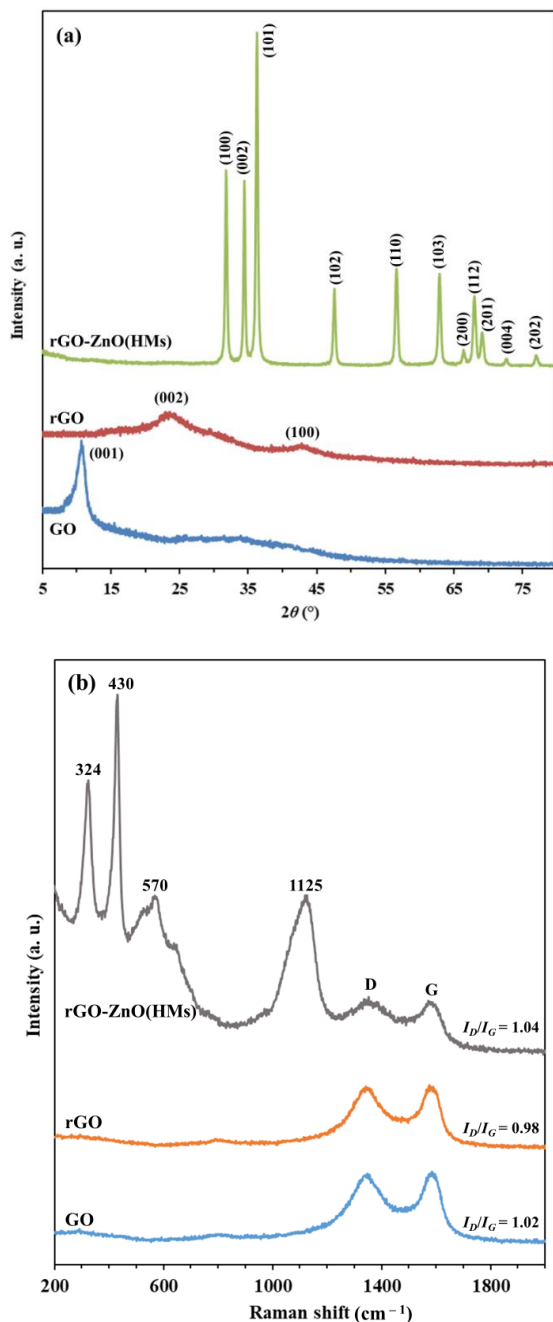


Figure 1. (a) XRD spectra and (b) Raman spectra for GO, rGO and rGO-ZnO(HMs) composite

XRD uses X-rays to analyse the crystalline structure of a material, revealing information about its composition and structure [19]. The rGO-ZnO(HMs) composite exhibits diffraction peaks at specific angles  $31.9^\circ$ ,  $34.5^\circ$ ,  $36.3^\circ$ ,  $47.6^\circ$ ,  $56.7^\circ$ ,  $62.9^\circ$ ,  $66.4^\circ$ ,  $67.9^\circ$ ,  $69.3^\circ$ ,  $72.5^\circ$  and  $77.0^\circ$ . These angles fit well with the hexagonal phase wurtzite of the ZnO structure, which is consistent with the reference pattern JPCDS 36-1451 [20]. No traces of impurities were detected, indicating that high-quality ZnO nanoparticles were synthesised. The

diffraction peaks exhibit high sharpness and intensity, indicating the formation of a well-crystalline structure of ZnO nanoparticles on the graphene surface. The absence of the GO peak implies that GO was completely reduced throughout the hybridisation process. The absence of rGO diffraction peaks in the rGO-ZnO(HMs) composite can be attributed to the extensive formation of ZnO and the comparatively low amount of rGO [18][21].

The presence of both carbon and ZnO in the structure of the prepared rGO-ZnO(HMs) composite can be confirmed from the Raman spectra. As shown in Figure 1(b), the characteristic Raman peaks of the rGO-ZnO(HMs) composite exhibit D and G bands at around  $1347\text{ cm}^{-1}$  and  $1589\text{ cm}^{-1}$ , respectively. The G band provides useful information on in-plane stretching vibrations of symmetric  $sp^2$  C-C bonds, while the D band is associated with the disturbance of the hexagonal graphitic lattice [22][23]. Compared with rGO, the D and G bands in the rGO-ZnO(HMs) composite were blue-shifted by  $5\text{ cm}^{-1}$  and  $14\text{ cm}^{-1}$ , respectively. These shifts are assigned to the chemical interaction between ZnO and rGO, which suggests that the electronic structure of the rGO could be modified by contacting it with ZnO nanoparticles [17]. The intensity ratio of these two  $I_D/I_G$  peaks is proportional to the disorder degree or structural defects located in the graphitic structure [24]. The calculated  $I_D/I_G$  ratios for GO, rGO and the rGO-ZnO(HMs) composite are 1.02, 0.98, and 1.04, respectively. The  $I_D/I_G$  ratio of rGO is smaller than that of GO, which suggests an increase in the average size of the in-plane  $sp^2$  domains upon reduction of GO. The relatively high  $I_D/I_G$  ratio for GO is contributed by the presence of oxygenated functional groups on both sides and edges of the GO sheets [25].

However, the rGO-ZnO(HMs) composite exhibits the highest  $I_D/I_G$  ratio due to the increasing disorder of  $sp^2$  domains contributed by the presence of ZnO nanoparticles on the graphene sheets. The rGO-ZnO(HMs) composite curve displayed four distinctive Raman vibration modes centred at  $324\text{ cm}^{-1}$ ,  $430\text{ cm}^{-1}$ ,  $570\text{ cm}^{-1}$  and  $1125\text{ cm}^{-1}$ , which are referred to as the ZnO spectrum. The edge at about  $324\text{ cm}^{-1}$  has been assigned to the second order Raman scattering ( $E_2$  (high)- $E_2$  (low) mode) and arises from the zone-boundary phonon of hexagonal ZnO [26]. The intense peak at  $430\text{ cm}^{-1}$  corresponds to the nonpolar optical phonon  $E_2$  (high) mode, which is known as the Raman active optical phonon mode and is related to the motion of oxygen atoms [23][27]. The

presence of the  $E_2$  (high) mode in the composite samples, which is characteristic of wurtzite hexagonal phase ZnO is consistent with the above XRD analysis. The peak at  $570\text{ cm}^{-1}$  is assigned to the  $E_1$  longitudinal optical ( $E_1(\text{LO})$ ) mode, attributed to oxygen deficiency defects in ZnO [26]. The broad band at  $1125\text{ cm}^{-1}$  is due to the multiple-phonon scattering processes ( $2A_1(\text{LO})$ ,  $2E_1(\text{LO})$  and  $2\text{LO}$  mode), characteristic of the II-IV semiconductor [23].

Scanning electron microscopy (SEM) is a standard technique for analyzing the surface structure and physical features of materials [28]. The surface morphology of the as-prepared rGO-ZnO(HMs) composite was analysed using FESEM. Homogeneous ZnO hollow microspheres were discovered to anchor the graphene structure (Figure 2(a)). The microspheres exhibited a size range of 800 to 1200 nm and were evenly dispersed across the graphene surface. The high-magnification image (Figure 2(b)) confirms that the microspheres consist of ZnO nanoparticles with a diameter of approximately 30 nm, which aligns with the results obtained from XRD analysis. TEM was employed to study the structure of the ZnO hollow microspheres that were formed on the surface of graphene. The observation that the central region of the microsphere has a lower density than the outer edge provides unambiguous evidence of the hollow interiors of the unique ZnO microspheres (Figure 2(c)).

### Formation mechanism of rGO-ZnO(HMs) composite

The process by which ZnO hollow microspheres are formed on graphene sheets is shown in Figure 3. The surface and edges of GO structure are rich in epoxide, hydroxyl, carbonyl and carboxyl acid reactive groups. The functional groups form C–O–Zn bonds to immobilise  $\text{Zn}^{2+}$  ions, leading to condensation reactions, enabling  $\text{Zn}^{2+}$  to be connected to these nucleation sites and ZnO quantum dots grown on graphene sheets by normal ionic bonds [29]. The elevated temperature within the autoclave induces the nucleation and subsequent growth of ZnO quantum dots to form nanoparticles. Simultaneously, due to the high temperature condition, ethanol can efficiently eliminate most of the oxygen-functional groups and reinstate the conjugated network of the graphitic lattice of GO, leading to the formation of rGO [30]. The ZnO nanoparticles preferentially aggregate and self-assemble into metastable spheres by the well-known growth mechanism of “oriented attachment” to minimise the total surface energy [31].

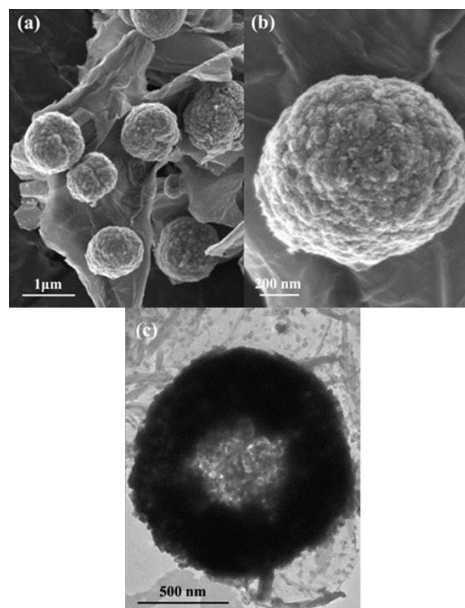


Figure 2. FESEM images of (a) rGO-ZnO(HMs) composite and (b) rGO-ZnO(HMs) composite with high-magnification; (c) TEM images of a single ZnO hollow sphere

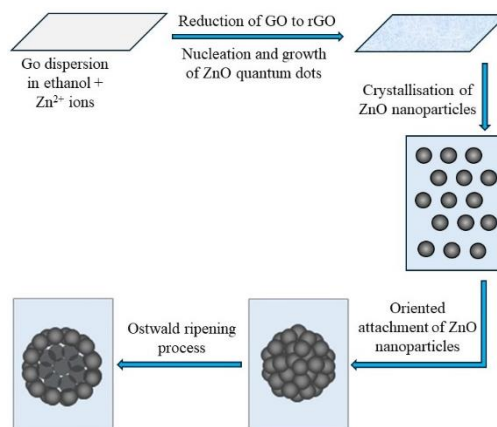


Figure 3. Schematic of the formation mechanism of ZnO hollow microsphere on rGO sheet

During an extended solvothermal process, the inner phase of metastable ZnO microspheres with higher energy will migrate to the stable outer surface through Ostwald ripening, leading to the formation of a hollow structure.

### Electrochemical Characteristics

Cyclic voltammetry (CV) is a widely recognised electrochemical method used to investigate the capacitive characteristics of a material. Figure 4(a) compares the CV profiles of rGO and rGO-ZnO(HMs) at a scan rate of 1 mV/s. The CV curves have an irregular quasi-rectangular shape without any distinct pair of redox peaks during both the anodic and cathodic

sweeps, indicating that capacitance is driven by a combination of electric double-layer capacitors (EDLCs) and faradaic redox activities. At the identical scanning rate, the rGO-ZnO(HMs) composite electrode exhibited a greater integrated area compared to the rGO electrode, confirming improved charge storage ability. The deposition of ZnO hollow microspheres on the surface of rGO significantly increases the total capacitance of the electrode. The specific capacitance,  $C_{sp}$  of the samples can be determined from the CV curves using (1) [25].

$$C_{sp} = (fi)/(m * s) \quad (1)$$

where  $fi$  is the integrated area of the CV curve,  $m$  is the mass of the electrode material in grams and  $s$  is the scan rate in volts per second. At a scan rate of 1 mV/s, the determined  $C_{sp}$  values for the rGO-ZnO(HMs) were 40.7 F/g, while the rGO had a  $C_{sp}$  value of 10.9 F/g.

The rGO-ZnO(HMs) composite electrode exhibits an almost four-fold increase in specific capacitance compared to the rGO electrode. This is attributed to the presence of nano-sized ZnO pseudocapacitance within the hollow microspheres that are adorned on the surface of rGO [14]. The CV curves of the rGO-ZnO(HMs) electrode were analysed at different scan rates to learn more about its capacitive behaviour (Figure 4(b)). The specific capacitance of the rGO-ZnO(HMs) electrode was determined at scan rates of 1, 10, 30, 50, 70, and 100 mV/s. The corresponding values were found to be 40.7, 32.3, 16.3, 11.0, 8.8, and 7.4 F/g, respectively.

The specific capacitance decreases significantly as the scan rates increase (Figure 4(c)), which is due to the limited time available for ion diffusion and adsorption within the intrinsic pore structures of the active material at high scan rates. This phenomenon of diffusion limits the passage of electrolytic ions, making certain active surface areas unavailable for storing electrical charge [16].

The electrodes' electrochemical performance was subsequently examined by a galvanostatic charge-discharge (GCD) test, which involved applying a sequence of charging and discharging currents to the electrochemical capacitors. At a constant current density of 1.00 A/g (Figure 5(a)), the galvanostatic charge-discharge diagram displays an almost symmetrical triangular form, with a small curvature in the charging curve for the rGO electrode.

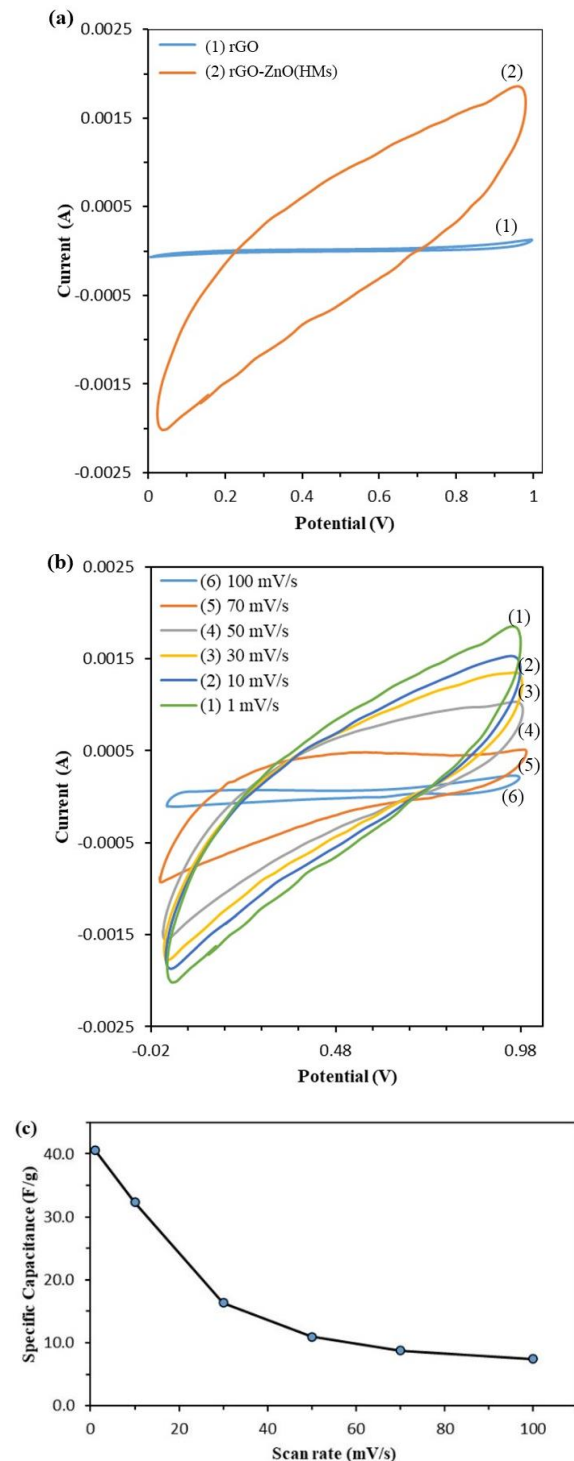


Figure 4. CV curves of (a) rGO and rGO-ZnO(HMs) at a scan rate of 1 mV/s, (b) rGO-ZnO(HMs) at different scan rates, and (c) variation of specific capacitance of rGO-ZnO(HMs) at different scan rates

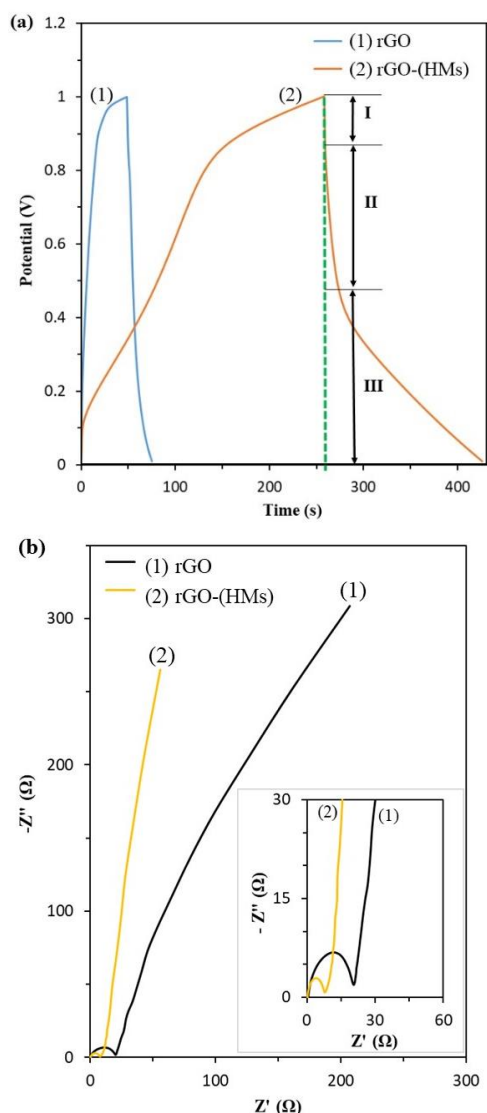


Figure 5. (a) Galvanostatic charge-discharge curves at a current density of 1.00 A/g and (b) Nyquist plots at 10 mV of rGO and rGO-ZnO(HMs) composite electrodes

This curvature suggests the presence of electric double layer capacitive behaviour. Meanwhile, the rGO-ZnO(HMs) composite curve deviates significantly from the triangular form, indicating the involvement of the ZnO Faradaic reaction process. This composite curve illustrates three potential variations in the discharge range. The sudden drop in current at the beginning of discharge is due to the internal resistance of the electrode (region I). The linear change in the potential over time indicates the behaviour of double-layer capacitance (region II), which is caused by the separation of charges at the electrode-electrolyte interface. The change in slope of the potential over time (region III) indicates the typical behaviour of pseudo-

capacitance, which occurs due to electrochemical adsorption/desorption or a redox reaction at the electrode-electrolyte interface [32].

Accordingly, the specific energy,  $E_{sp}$  and specific power,  $P_{sp}$  were calculated from the GCD data using the equations:

$$E_{sp} = (CV^2)/2m \quad (2)$$

$$P_{sp} = E_{sp}/t \quad (3)$$

where  $C$  is specific capacitance estimated from charge-discharge curves,  $V$  is the potential range during discharge,  $t$  is the discharge time and  $m$  is the total mass of electroactive material of the electrodes. Their maximum values are tabulated in Table 1.

Utilising electrochemical impedance spectroscopy (EIS) to analyse the resistive behaviour of electrode materials is a beneficial method. Figure 5(b) displays the Nyquist plots of the rGO and rGO-ZnO(HMs) composite electrodes at a voltage of 10 mV. The semicircles observed in the high-frequency range represent the electronic resistance in the electrode materials caused by the charge transfer occurring at the electrode/electrolyte interface. Meanwhile, the ion diffusion in the electrolyte is represented by the steeply rising straight line in the low-frequency region. The equivalent series resistance (ESR) is determined at the point where the semicircle initially intersects the x-axis. The intersection signifies the total resistance resulting from the combination of the bulk electrolyte, electrode, and the contact resistance between the electrode and current collector [33]. The faradaic charge transfer resistance,  $R_{ct}$  can be determined by measuring the diameter of the semicircle arc on the real axis [34]. The semicircle with a reduced diameter facilitates efficient electron transmission between the electrode material and the electrolyte. Table 1 shows the ESR and  $R_{ct}$  values calculated from the Nyquist plot in Figure 5(b) for the rGO and rGO-ZnO(HMs) composite electrodes. The higher ESR and  $R_{ct}$  values of the rGO electrode strongly suggest that attaching ZnO hollow microspheres to the surface of graphene sheets increases charge transfer.

Table 1. Electrochemical parameters of rGO and rGO-ZnO(HMs) composite electrodes

Sample	ESR (Ω)	R <sub>ct</sub> (Ω)	Specific Capacitance C <sub>sp</sub> (F/g)	Energy Density E <sub>sp</sub> (Wh/kg)	Power Density P <sub>sp</sub> (kW/kg)
rGO	0.49	20.01	10.9	0.81	0.63
rGO-ZnO(HMs)	0.38	7.55	40.7	5.75	1.79

## CONCLUSION

The rGO-ZnO(HMs) composite was synthesised as an electrode material for supercapacitors using a one-step solvothermal technique. A comprehensive investigation has been conducted on the physical and electrochemical behaviour of the composite material. The FESEM and TEM images showed that ZnO hollow microspheres were uniformly distributed over the rGO sheet substrate. The microspheres are composed of ZnO nanoparticles with a diameter of around 30 nm. The rGO-ZnO(HMs) composite synthesized at a concentration of 0.25 mM zinc precursor exhibited the highest specific capacitance of 40.7 F/g at a scan rate of 1 mV/s, with energy and power densities of 5.75 W h/kg and 1.79 kW/kg, respectively.

## ACKNOWLEDGMENT

Financial support has been gratefully acknowledged from the Universiti Pertahanan Nasional Malaysia (UPNM) Geran Penyelidikan Jangka Pendek (UPNM/2020/GPJP/SG/6) and the Malaysian Ministry of Higher Education (MOHE).

## REFERENCES

- [1] T. Tene et. al., "Optical properties of graphene oxide," *Frontiers in Chemistry*, vol. 11, no. 1214072, pp. 1-14, 2023, doi: 10.3389/fchem.2023.1214072
- [2] G. Jing, et. al., "Introducing reduced graphene oxide to enhance the thermal properties of cement composites," *Cement and Concrete Composites*, vol. 109, no. 103559, pp. 1-10, 2020, doi: 10.1016/j.cemconcomp.2020.103559
- [3] A. Osman, et. al., "Thermal, electrical and mechanical properties of graphene/nano-alumina/epoxy composites," *Materials Chemistry and Physics*, vol. 257, no. 123809, pp. 1-11, 2020, doi: 10.1016/j.matchemphys.2020.123809
- [4] L. Ding, et. al., "Covalently bridging graphene edges for improving mechanical and electrical properties of fibers," *Nature Communications*, vol. 15, no.4880, pp. 1-10, 2024, doi: 10.1038/s41467-024-49270-5
- [5] A. Mallik, et. al., "Single step synthesis of reduced graphene oxide/SnO<sub>2</sub> nanocomposites for potential optical and semiconductor applications," *Materials Science and Engineering: B*, vol. 264, no. 114938, pp. 1-10, 2020, doi: 10.1016/j.mseb.2020.114938
- [6] H. E. Marouazi, et. al., "Few Layer Graphene/TiO<sub>2</sub> Composites for Enhanced Solar-Driven H<sub>2</sub> Production from Methanol," *ACS Sustainable Chemistry & Engineering*, vol. 9(10), pp. 3633-3646, 2021, doi: 10.1021/acssuschemeng.0c06808
- [7] J. Azuaje, et. al., "Catalytic performance of a metal-free graphene oxide-Al<sub>2</sub>O<sub>3</sub> composite assembled by 3D printing," *Journal of the European Ceramic Society*, vol. 41, no. 2, pp. 1399-1406, 2021, doi: 10.1016/j.jeurceramsoc.2020.10.010
- [8] K. Y. Chen, et. al., "Reduced graphene oxide/Fe<sub>2</sub>O<sub>3</sub> hollow microspheres coated sponges for flexible electromagnetic interference shielding composites," *Composites Communications*, vol. 23, no. 100572, pp. 1-7, 2021, doi: 10.1016/j.coco.2020.100572
- [9] H. Han, et. al., "Binder assisted self-assembly of graphene oxide/Mn<sub>2</sub>O<sub>3</sub> nanocomposite electrode on Ni foam for efficient supercapacitor application," *Ceramics International*, vol. 46, 10A, pp. 15631-15637, 2020, doi: 10.1016/j.ceramint.2020.03.111
- [10] L. Yu, et. al., "Synthesis of ZnO core/shell hollow microspheres to boost light harvesting capability in quantum dots-sensitized solar cell," *Chemical Physics Letters*, vol. 764, no. 138283, pp. 1-6, 2021, doi: 10.1016/j.cplett.2020.138283
- [11] Y. Ma, et.al., "Hollow multishelled structural ZnO fillers enhance the ionic conductivity of polymer electrolyte for lithium batteries," *Journal of Nanoparticle Research*, vol. 25, no. 14, pp. 1-11, 2023, doi: 10.1007/s11051-022-05661-7
- [12] L. Zhou, et. al., "Template-free synthesis and photocatalytic activity of hierarchical hollow ZnO microspheres composed of radially aligned nanorods," *Journal of Physics and Chemistry of Solids*, vol. 148, no. 109719, pp. 1-8, 2021, doi: 10.1016/j.jpcs.2020.109719
- [13] S. Wang, et.al., "Synthesis of ZnO Hollow Microspheres and Analysis of Their Gas Sensing Properties for n-Butanol," *Crystals*, vol. 10(11), no. 1010, pp. 1-11, 2020, doi: 10.3390/cryst10111010
- [14] A. L. Albert, et. al., "Physical and Electrochemical Properties of Graphene Decorated with ZnO Hollow Spheres for Supercapacitor Applications," *Key Engineering Materials*, vol. 908, pp. 284-292. 2022, doi: 10.4028/p-759prg
- [15] V. Puspasari, et. al., "ZnO-based antimicrobial coatings for biomedical

- applications," *Bioprocess and Biosystems Engineering*, vol. 45, pp. 1421-1445, 2022, doi: 0.1007/s00449-022-02733-9
- [16] A. Ramadoss and S. J. Kim, "Improved activity of a graphene-TiO<sub>2</sub> electrode in an electrochemical supercapacitor," *Carbon*, vol. 63, pp. 434-445, 2013, doi: 10.1016/j.carbon.2013.07.006
- [17] F.S. Omar, et. al., "Microwave Synthesis of Zinc Oxide/Reduced Graphene Oxide Hybrid for Adsorption-Photocatalysis Application," *International Journal of Photoenergy*, vol. 2014, no. 176835, pp. 1-9, 2014, doi: 10.1155/2014/176835
- [18] T. Lv, et. al., "Enhanced photocatalytic degradation of methylene blue by ZnO-reduced graphene oxide composite synthesized via microwave-assisted reaction," *Journal of Alloys and Compounds*, vol. 509(41), pp. 10086-10091, 2011, doi: 10.1016/j.jallcom.2011.08.045
- [19] N. A. Khairulazman, et. al., "Mineralogical analysis of plutonic and volcanic rocks at selected slope sections of the Kuala Lumpur-Karak Highway," *Sinergi*, vol. 29, no.1, pp. 259-267, 2025, doi: 10.22441/sinergi.2025.1.024
- [20] M. P. Ramike, et. al., "Exploration of the Different Dimensions of Wurtzite ZnO Structure Nanomaterials as Gas Sensors at Room Temperature," *Nanomaterials*, vol. 13(20), no. 2810, pp. 1-22, 2023, doi: 10.3390/nano13202810
- [21] R. Gang, et. al., "Facile One-step Production of 2D/2D ZnO/rGO Nanocomposites under Microwave Irradiation for Photocatalytic Removal of Tetracycline," *ACS Omega*, vol. 6, no. 5, pp. 3435-4110, 2021, doi: 10.1021/acsomega.0c05559
- [22] I. Tanisik, et. al., "Solar-hydrogen production with reduced graphene oxide supported Cd<sub>x</sub>Zn<sub>1-x</sub>S photocatalysts," *International Journal of Hydrogen Energy*, vol. 45, no. 60, pp. 1-12, 2020 doi: 10.1016/j.ijhydene.2020.04.035
- [23] S. S. Low, et. al., "Sensitivity enhancement of graphene/zinc oxide nanocomposite-based electrochemical impedance genosensor for single stranded RNA detection," *Biosensors and Bioelectronics*, vol. 94, pp. 365-373, 2017, doi: 10.1016/j.bios.2017.02.03
- [24] L. Stan, et. al., "Intense Blue Photo Emissive Carbon Dots Prepared through Pyrolytic Processing of Ligno-Cellulosic Wastes," *Nanomaterials*, vol. 13, no. 131, pp. 1-13, 2022, doi: 10.3390/nano13010131
- [25] S. P. Lim, et. al., "Solvothermal synthesis of SnO<sub>2</sub>/graphene nanocomposites for supercapacitor application," *Ceramics International*, vol. 39, no. 6, pp. 6647-6655, 2013, doi: 10.1016/j.ceramint.2013.01.102
- [26] P. Kumar, et. al., "Investigation of phase segregation in yttrium doped zinc oxide," *Ceramics International*, vol. 41, no. 5, pp. 6734-6739, 2015, doi: 10.1016/j.ceramint.2015.01.117
- [27] Z. A. Ali, et. al., "Green Synthesis of ZnO Nanostructures Using *Pyrus pyrifolia*: Antimicrobial, Photocatalytic and Dielectric Properties," *Crystals*, vol. 12, no. 1808, pp. 1-15, 2022, doi: 10.3390/cryst12121808
- [28] A. Kolakoti, et. al., "Preparation and mechanical characterization of natural polymer composite material obtained from fox tail palm seeds," *Sinergi*, vol. 28, no. 3, pp. 505-512, 2024, doi: 10.22441/sinergi.2024.3.007
- [29] Y. Li, et. al., "Recent Advances in Zinc Oxide Nanostructures with Antimicrobial Activities," *International Journal of Molecular Sciences*, vol. 21, no. 8836 pp. 1-70, 2020, doi: 10.3390/ijms21228836
- [30] Z. Wang, et. al., "The green synthesis of reduced graphene oxide by the ethanol-thermal reaction and its electrical properties," *Materials Letters*, vol. 116, pp. 416-419, 2014, doi: 10.1016/j.matlet.2013.11.081
- [31] C. X. He, et. al., "Sonochemical preparation of Hierarchical ZnO Hollow spheres for efficient dye-sensitized cells," *Chemistry: A European Journal*, vol. 16, no. 29, pp. 8757-8761, 2010, doi: 10.1002/chem.201000264
- [32] G. S. Gund, et. al., "Enhanced activity of chemically synthesized hybrid graphene oxide/Mn<sub>3</sub>O<sub>4</sub> composite for high performance supercapacitors," *Electrochimica Acta*, vol. 92, pp. 205-215, 2013, doi: 10.1016/j.electacta.2012.12.120
- [33] V. Sunil, et. al., "Characterization of supercapacitive charge storage device using electrochemical impedance spectroscopy," *Materials Today: Proceedings*, vol. 46, no. 4, pp. 1588-1594, 2021, doi: 10.1016/j.matpr.2020.07.248
- [34] N. O. Laschuk, et. al., "Reducing the resistance for the use of electrochemical impedance spectroscopy analysis in materials chemistry," *RSC Advances*, vol. 11, pp. 27925-27936, 2021, doi: 10.1039/d1ra03785d